NEOPLASIA
www.neoplasia.com

Volume 13 Number 7 July 2011 pp. 620–632 620

# Metabolic Targeting of Lactate Efflux by Malignant Glioma Inhibits Invasiveness and Induces Necrosis: An *In Vivo* Study[1]

**Chaim B. Colen*, Yimin Shen†, Farhad Ghoddoussi‡, Pingyang Yu*, Todd B. Francis*, Brandon J. Koch§, Michael D. Monterey*, Matthew P. Galloway‡, Andrew E. Sloan¶ and Saroj P. Mathupala#**

*Department of Neurological Surgery, Wayne State University School of Medicine, Detroit, MI, USA; †Department of Radiation Biology, Wayne State University School of Medicine, Detroit, MI, USA; ‡Departments of Psychiatry and Behavioral Neurosciences, and Anesthesiology, Wayne State University School of Medicine, Detroit, MI, USA; §Department of Biochemistry and Molecular Biology, Rollins College, Winter Park, FL, USA; ¶Department of Neurological Surgery, Case Western Reserve University School of Medicine, Cleveland, OH, USA; #Department of Neurological Surgery and Karmanos Cancer Institute, Wayne State University School of Medicine, Detroit, MI, USA

## Abstract

Glioblastoma multiforme (GBM) are the most malignant among brain tumors. They are frequently refractory to chemotherapy and radiotherapy with mean patient survival of approximately 6 months, despite surgical intervention. The highly glycolytic nature of glioblastomas describes their propensity to metabolize glucose to lactic acid at an elevated rate. To survive, GBMs efflux lactic acid to the tumor microenvironment through transmembrane transporters denoted monocarboxylate transporters (MCTs). We hypothesized that inhibition of MCT function would impair the glycolytic metabolism and affect both glioma invasiveness and survival. We examined the effect on invasiveness with α-cyano-4-hydroxy-cinnamic acid (ACCA, 4CIN, CHCA), a small-molecule inhibitor of lactate transport, through Matrigel-based and organotypic (brain) slice culture invasive assays using U87-MG and U251-MG glioma cells. We then conducted studies in immunodeficient rats by stereotaxic intracranial implantation of the glioma cells followed by programmed orthotopic application of ACCA through osmotic pumps. Effect on the implanted tumor was monitored by small-animal magnetic resonance imaging. Our assays indicated that glioma invasion was markedly impaired when lactate efflux was inhibited. Convection-enhanced delivery of inhibitor to the tumor bed caused tumor necrosis, with 50% of the animals surviving beyond the experimental end points (3 months after inhibitor exhaustion). Most importantly, control animals did not display any adverse neurologic effects during orthotopic administration of ACCA to brain through programmed delivery. These results indicate the clinical potential of targeting lactate efflux in glioma through delivery of small-molecule inhibitors of MCTs either to the tumor bed or to the postsurgical resection cavity.

*Neoplasia (2011) 13, 620–632*

Address all correspondence to: Saroj P. Mathupala, PhD, Department of Neurological Surgery & Karmanos Cancer Institute, Wayne State University School of Medicine, 607 HWCRC, 4100 John R., Detroit, MI 48201. E-mail: smathupala@med.wayne.edu

[1]Research support was provided by grants from the American Cancer Society IRG-85-003-14 (S.P.M.); LEARN Foundation, Mich (S.P.M.); the National Institutes of Health (CA116257 to S.P.M.); Marvin E. Klein, MD, Charitable Trust (S.P.M.); the Fund for Medical Research and Education, Wayne State University School of Medicine (C.C.); the Joe Young Fund for Research in Psychiatry (M.P.G.); and the Anesthesiology Fund for Medical Research (M.P.G. and F.G.). None of the authors of this article received any financial support in conjunction with the generation of this submission. None of the authors have a financial conflict of interest.
Received 8 January 2011; Revised 6 May 2011; Accepted 12 May 2011


DOI 10.1593/neo.11134

## Introduction

The most common type of malignant tumor that occurs in brain (primary brain tumors) is referred to as glioblastoma. Unfortunately, it is also the most lethal. Current data and projections indicate that, in the United States, an estimated 22,000 new cases of brain tumor will be diagnosed in 2010, whereas 13,000 deaths will occur due to the same (www.abta.org), a dismal statistic at best. Brain tumors are the second leading cause of cancer-related deaths in males up to age 39 and in females and children younger than 20 years. The incidence of primary brain tumors increases with age, peaking at ages 75 to 84 years.

The standard therapy for patients diagnosed with malignant brain tumors is surgical debulking (removal) of the tumor followed by radiotherapy and chemotherapy. Even with such multimodal interventions, the prognosis for patients remains dismal, with a mean survival of 6 to 12 months from the time of diagnosis. These discouraging facts clearly indicate a need for alternative approaches to target these tumors.

One such avenue is to attack the deviant metabolic pathways that are present in glioblastoma, a feature common to most highly malignant tumors. Primarily, such tumors have the propensity to consume copious amounts of glucose at a rapid rate and convert most of it to lactic acid, even in the presence of ample oxygen [1–5]. Termed "aerobic glycolysis," this metabolic phenotype markedly contrasts with that observed in normal tissues, where glycolysis (conversion of glucose to lactic acid) primarily occurs under hypoxic conditions. To maintain the enhanced glycolytic flux, glioblastomas need to rapidly efflux lactic acid to the tumor microenvironment, which is facilitated by a set of plasma membrane transporters denoted monocarboxylate transporters (MCTs) [6]. Although 14 isoforms of MCTs have been identified during *in silico* analysis of the human genome, only four (MCTs 1-4) are known to play a role in lactic acid transport in mammalian tissues, including tumors [7].

Previous studies by us [8] and others [9–12] have demonstrated differential expression of MCT isoforms in brain tumors in contrast to normal brain tissue. *In vitro* studies that used RNA interference to target brain tumor–expressed MCT isoforms to selectively interfere with lactate efflux also resulted in altered intracellular pH changes and tumor cell death [8]. Our *in vitro* studies and those of others [13–16] have shown that inhibition of lactate transport in tumors with α-cyano-4-hydroxycinnamic acid (abbreviated as ACCA, α-CCA, 4CIN, or as CHCA; $M_W$ = 189.2), a small-molecule competitive inhibitor of mammalian lactate transporters [17], can cause growth inhibition of tumors or tumor cell death. Furthermore, we [13] and others [18,19] have shown that application of ACCA will impact tumor metabolism to enhance its radiosensitivity by up to 10-fold.

We hypothesized that disruption of lactate efflux through application of ACCA directly to the tumor mass (*in vivo*) or to the tumor microenvironment should either halt or significantly inhibit the tumor's growth and capacity to invade the surrounding normal brain tissues. We hoped that targeting glycolysis will impact the overall energy balance of the tumor that is crucial for tumor survival, and in turn, adversely affect the tumor to eventually cause tumor necrosis. However, we were concerned that such an approach *in vivo* may also negatively impact normal brain function because of the interference with lactate shuttling that occurs between neurons and surrounding astrocytes during neuronal "firing," a recently recognized metabolic phenomenon in normal brain [20,21].

To clarify these issues and to evaluate the utility of small-molecule inhibitors of MCTs as therapeutic tools for metabolic targeting of brain tumors, we first investigated the affect of inhibiting lactate efflux in glioblastoma on their invasiveness through Matrigel-based *in vitro* invasion assays [22,23] and then with organotypic brain slice culture assays [24,25]. On the basis of the distinct inhibition of invasiveness observed on the presence of ACCA in the growth medium, we conducted *in vivo* studies in an orthotopic brain tumor nude rat model (Crl: NIH-rnu) using convection-enhanced delivery (CED) of ACCA to the tumor bed. The results indicated marked inhibition of tumor growth *in vivo*, including complete necrosis of tumor tissue in most of the experimental animals, with no recurrence of tumor once the chemical was exhausted. We also analyzed select metabolic profiles of normal brains of control animals subjected to the same therapeutic dosages of ACCA to test for toxicity or adverse metabolic effects. Analysis of ACCA concentration gradients across brain of the nude rat model indicated that pharmacologically relevant ACCA concentrations were sufficient to cause complete necrosis of the tumor.

## Materials and Methods

### *Cell Lines, Reagents, and Culture Media*

Human glioblastoma cell lines U87-MG and U251-MG were obtained from the American Type Culture Collection (Manassas, VA) and maintained in Dulbecco modified Eagle medium/F-12 medium (DMEM/F12) supplemented with 10% fetal bovine serum and the antibiotic gentamicin. Media and reagents were purchased from Invitrogen (Carlsbad, CA). Fetal bovine serum was obtained from Atlanta Biologicals (Atlanta, GA). Basal DMEM (glucose-, glutamine-, phenol red–, and glutamine-free) was obtained from Mediatech, Inc (Manassas, VA).

### *Enhanced Green Fluorescent Protein Expressing Glioma Cells*

The two glioma cell lines were engineered to express enhanced green fluorescent protein (EGFP) for use in the invasion assays described herein. In brief, EGFP complementary DNA was amplified with polymerase chain reaction from the plasmid EGFP-N1 (Clontech, CA) and cloned into the *Eco*RI and *Xho*I restriction sites of a bicistronic retroviral expression vector pLXRN [26]. Recombinant retrovirions were generated through the PA317 amphotropic packaging cell line using established protocols [27,28]. Glioma cells were transduced with the retrovirions at a multiplicity of infection of 10 in the presence of 8 μg/ml polybrene and passaged in the presence of geneticin (G-418; 0.75 mg/ml) until 100% of the cells expressed EGFP as observed by fluorescence microscopy (fluorescein isothiocyanate filter; excitation, 480 nm; emission, 535 nm).

### *Reagent Preparations*

Stock solutions of 0.1 M α-cyano-4-hydroxycinnamic acid (ACCA) were prepared in basal DMEM and the pH was adjusted to 7.4 with NaOH. Stock solutions of pyruvate, lactate, or glucose (50 mM) were also prepared in basal DMEM (pH 7.4). All solutions were filter sterilized using 0.22-μm syringe-filter units (Millex-GV, Molheim, France).

### *Oxygen Consumption Assay*

U87-MG glioma cells maintained in complete DMEM/F12 medium were detached with Accutase (an invertebrate-derived cell detachment solution; Innovative Cell Technologies, San Diego, CA), washed once in complete DMEM/F12 medium, and were resuspended at $0.5 \times 10^5$ cells/μl in the same medium. An oxygen electrode (Mitocell 200A; Strathkelvin Instruments, Glasgow, UK) equipped with a fast-response fluorinated ethylene propylene membrane was

used to measure $O_2$ consumption at 25°C. In brief, the electrode was calibrated with air-saturated water (high-point, 267 μM) and 2% (wt/vol) $Na_2SO_3$ in 0.01 M $Na_3BO_3$ buffer (zero point). Respiration rates were measured in 10-minute intervals first with $0.5 \times 10^6$ cells resuspended in 200 μl of DMEM/F12 medium, followed by addition of 10 mM ACCA (20 μl of 0.1 M ACCA). Then, 5 μl of 1.6 mM digitonin was added to permeabilize the cell membranes. The ACCA and digitonin concentrations used were as described by us previously [13].

### *Matrigel-Based Invasion Assay*

Twenty-four-well tissue culture plates (Falcon; BD Biosciences, Bedford, MA) and fluorescence blocking well inserts (Falcon HTS FluoroBlok Inserts; pore size, 8 μm; growth area, 0.3 $cm^2$) were used for the assays. Matrigel (8 mg/ml; BD Biosciences) was diluted 1:3 in basal DMEM supplemented with 2 mM glutamine. Twenty-microliter aliquots of Matrigel suspension were applied to the FluoroBlok well inserts placed in each well and allowed to set at 37°C. The inserts were then placed in the 24-well plates containing 0.75 ml of conditioned medium per well (medium from either subconfluent U87-MG or U251-MG cultures was used as the chemoattractant in the lower chambers). For the experiments, well inserts were supplemented with 0.5 ml of 1 mM pyruvate, 5 mM lactate, or 25 mM glucose medium that contained EGFP-expressing glioma cells ($4 \times 10^4$ cells). The pyruvate and lactate levels were chosen to represent levels that are also physiologically relevant. Glucose was used at five times the physiological levels to maintain a high-glycolytic flux across tumor cells. To test for invasion capacity of glioma on inhibition of MCTs, one set of samples contained 25 mM glucose in the well insert, whereas the spent medium in the lower chamber was supplemented with 10 mM ACCA. The pH of the samples was maintained at 7.4. Appearance of cells on bottom surface of well inserts was monitored through fluorescence microscopy. After 48 hours, fluorescence of the top and bottom surfaces of the inserts was quantified using a fluorescent plate reader (Tecan-Ultra, Durham, NC), and the invasive capacity was calculated (fluorescence on bottom surface of insert/total fluorescence from both surfaces of insert).

### *Organotypic (Brain) Slice Culture Invasion Assay*

All animal experiments were done according to institutionally approved animal protocol guidelines. Nude rats, weighing 450-500 g, were anesthetized intraperitoneally with a mixture of ketamine (90 mg/kg) and xylazine (10 mg/kg), and the skull was exposed under sterile conditions. The spinal column was severed with a sharp scalpel, and a midsagittal cut was made along the skull to expose the brain. The brains were rapidly extracted, washed in cold (4°C) basal DMEM and placed in a 0.5-mm coronal rat brain matrix (Braintree Scientific, Braintree, MA) bathed in basal DMEM. Brain slices were obtained using tissue slicer blades (Thomas Scientific, Swedesboro, NJ) and separated into sterile dishes. Tissue disks, 8 mm in diameter, were obtained from the slices using disposable dermal biopsy punches (Miltex, York, PA) and expirated into FluoroBlok well inserts filled with basal DMEM. The medium was then carefully aspirated to settle the brain slices on to the insert's membrane. Any irregular gaps between the brain slice and the wall of the well insert were sealed with 5 to 10 μl of Matrigel prepared as described and allowed to set. EGFP-expressing glioma cells ($4 \times 10^4$ cells) were placed on top of the brain slices in 50 μl of basal DMEM as a cushion and allowed to incubate for 30 minutes. Well inserts were then supplemented with 0.5 ml of 1 mM pyruvate, 5 mM lactate, or 25 mM glucose. Conditioned medium (0.75 ml per well, from glioma cultured DMEM containing 10% fetal bovine serum) was used as a chemoattractant in the lower chambers. To test for invasion capacity of glioma when lactate transport is inhibited, a set of samples contained 25 mM glucose in the well insert, whereas the spent medium in the lower chamber was supplemented with 10 mM ACCA. After 120 hours, fluorescence of the top and bottom surfaces of the inserts was quantified using a fluorescent plate reader (Tecan-Ultra), and the invasive capacity was calculated (fluorescence on bottom surface of insert/total fluorescence from both surfaces of insert). Aliquots of brain slices maintained in separate wells were withdrawn from culture every 24 hours, and their viability was tested using trypan blue exclusion assays. For this, brain slice fragments were dispersed with Accutase at room temperature, and the suspensions were tested for viability. The brain slices maintained a minimum of 95% viability throughout the duration of the invasion assay experiments.

To quantify fluorescence on top surface of well inserts, the spent medium was aspirated and the wells were gently rinsed with 0.5 ml of phosphate-buffered saline (PBS). A 4500-μm well border was assigned in the plate reader software to read the well insert surface only, in a 9 × 9 filled circle matrix. Excitation and emission wavelengths used were 485 and 520 nm, respectively (preset manual gain of 100). The plates were read without lids to prevent background light scattering. Sham well inserts with either Matrigel or brain slices were used to compensate for background fluorescence. To read the bottom surface, the inserts were briefly dipped in 0.5 ml of PBS, the plastic placeholder flanges were snipped off, and the inserts were placed inverted in a fresh 24-well plate. The bottom surfaces were read using the same parameters as for the top surfaces. The above procedures were followed to minimize fluorescence quenching and background effects by both the culture medium and the ACCA.

### *Intracranial Implantation of U87-MG Glioma in a Nude Rat Model*

An orthotpic xenograft nude rat model (Crl: NIH-rnu; Charles River Laboratories, Wilmington, MA) was used in this study. In brief, 8- to 10-week-old (250-300 g) male rats were anesthetized as before and immobilized on a rodent stereotaxic device (Kopf Instruments, Tujunga, CA). The surgical zone was prepared with povidone-iodine according to approved animal protocols, a 1-cm incision was made retro-orbitally along the sagittal plane, and the skull was exposed. A burr hole (without penetrating the dura) was created 2 mm lateral to the bregma and 1 mm anterior to the coronal suture [29]. U87-MG glioma cells ($1 \times 10^6$ cells suspended in 10 μl of PBS supplemented with 25 mM glucose) were inoculated into the caudate-putamen (CPu) region. The glioma cells were slowly injected at a depth of 5 mm from the skull using a Hamilton syringe (10 μl, Model 80301) fitted with a 27-gauge needle (tapered end directed toward midline), positioned with a syringe attachment fitted to the stereotaxic device. After 5 minutes, the needle was slowly withdrawn, and the skin incision was first sutured closed and then approximated with Dermabond (Closure Medical Corporation, Raleigh, NC).

### *Programmed Orthotopic Delivery of ACCA to the Tumor Bed*

Fourteen days after tumor implantation, the animals were imaged by magnetic resonance imaging (MRI) to visualize the bulk tumor. The animals were anesthetized under sterile conditions as described previously, and the previous surgical site was reexposed. A nonmetallic (MRI-compatible) brain infusion cannula made of silica (5 mm in length, 0.36 mm in diameter; catalog no. 328OP/FS; Plastics One, Roanoke, VA) was connected through a 3-cm-long polyethylene tube

to an osmotic pump (200-μl capacity, with a 28-day delivery period [catalog no. 2004; 0.25 μl/h]; Alzet, Cupertino, CA). The pumps were primed with saline (control animals) or with either 20 or 40 mM ACCA in PBS buffered to pH 7.4 (test animals). The cannula was lowered through the previous burr hole to the same depth as for the tumor inoculation to "hit" the tumor core. The cannula was then sealed to the skull with cyanoacrylate adhesive (Loctite 454; Loctite Corp, Rocky Hill, CT). The osmotic pump was inserted into a subcutaneous cavity created in the midscapular region. Afterward, the entire surgical area was flushed with saline before suturing of the skin incision, followed by application of Dermabond to seal the scalp.

### *Magnetic Resonance Imaging*

MRI of the tumor-implanted nude rats was carried out at the MR Research Facility, Wayne State University in a Bruker Biospec AVANCE small-animal imager (Bruker Instruments, Billerica, MA) equipped with a 4.7-T horizontal bore magnet. Brain images were acquired using T1- and T2-weighted scans. MRI was performed to confirm intracranial tumor growth 1) before orthotopic placement of cannulae coupled to either saline- or ACCA-primed osmotic pumps (described above) and 2) subsequently, to monitor tumor growth or regression. Before imaging, each animal was anesthetized by intraperitoneal injection of ketamine and xylazine (as described under surgical procedures) to prevent animal movement within the magnet during imaging. 0.3 mmol/kg of gadopentate dimeglumine (Magnevist, Berlex Laboratories, Montville, NJ) was applied through tail vein catheterization for contrast enhancement. A receive-only surface coil (30 mm in diameter) was placed over the skull area, and the animal was placed in the magnetic coil (72 mm in diameter) for the procedure. Two-dimensional multislice T2-weighted and T1-weighted fast-spin echo sequences were used to acquire coronal and sagittal images of each animal. Each imaging run was completed within 5 minutes. The initial image was obtained 14 days after implantation of tumor to verify tumor growth. The second image was obtained after cannulation of the tumor. The surviving animals were imaged again at 28 days (14 days after osmotic pump application) and then again at 56 and 120 days.

### *Experimental End Points*

Both control (saline) and test (ACCA) animals were provided food and water *ad libitum*, and maintained under sterile conditions. Tumor shrinkage or growth was monitored by MRI as described above. Animals were removed from the experiment 1) at 120 days after tumor implantation or 2) because of pain or trauma (due to excessive tumor growth). The animals were imaged again at experimental end points and killed by $CO_2$ narcosis followed by bilateral pneumothorax. After sacrifice, brains were rapidly recovered by making a sagittal excision along the dorsal surface of the skull, and placed in formalin (4% vol/vol) buffered with PBS. The fixed tissues were paraffin-embedded and sectioned in 2-μm coronal slices both anterior and posterior to the cannula implantation site, and the slices were processed for histology (hematoxylin and eosin [H&E] staining).

### *Analysis of ACCA Diffusion during CED in the Orthotopic Nude Rat Model*

The same stereotaxic coordinates as described above for tumor implantation were used in this procedure using 28-day Alzet osmotic pumps primed with saline or 40 mM ACCA in PBS (pH 7.0). The cannulae were implanted into the CPu region in 300- to 350-g nude rats ($n$ = 4 per group). The animals were provided food and water *ad libitum* and monitored for 2 weeks for any weight loss or adverse neurologic symptoms (including gait, grooming, and response to handling). At the end of 2 weeks, the animals were killed by $CO_2$ narcosis, and brains were removed intact. Brains were immediately placed in a 0.5-mm coronal brain matrix (Braintree Scientific), and 1.0-mm-thick coronal slices were excised anterior to—and posterior to—the cannulation site. These were then weighed and stored at −80°C until processed for high-performance liquid chromatography–mass spectrometry (HPLC-MS) analysis (described below) to quantify ACCA concentrations in each slice.

The extraction and analysis of ACCA were carried out at the on-site pharmacology core facility at Karmanos Cancer Institute. Immediately before analysis, each slice was thawed in a water bath at ambient temperature and homogenized in 1.0 ml of 10 mM ammonium formate (pH 7.5) using a micropestle device (Fisher Scientific, Hanover Park, IL). The homogenates were extracted in ethyl acetate and resolved by HPLC (Xterra MS C18 3.5-μm column, 2.1 × 50 mm) with 70% methanol/ 10 mM ammonium formate, pH 7.5, as the elution buffer on a separation system (Model 2695; Waters, Milford, MA). Prepared standards of ACCA in same buffer were used to calculate the concentration of ACCA in the brain slices with Zileuton (*N*-(1-benzobthien-2-ylethyl)-*N*-hydroxyurea)) (Rhodia Pharma Solutions Ltd, Cramlington, UK) as the internal standard [30]. Drug-free (blank) rat plasma was obtained from Innovative Research, Dearborn, Mich. ACCA in the eluates were detected using a Waters Quattro Micro triple quadrupole mass spectrometric detector equipped with an electrospray ionization source.

### *$^1$H Magnetic Resonance Spectroscopic Analysis of Metabolic Changes in Brain on CED of ACCA*

To ascertain possible metabolic changes in the brain of the experimental animals, we delivered saline or 40 mM ACCA through CED to the same stereotaxic coordinates as before using 200- to 250-g nude male rats ($n$ = 2 per group). Two weeks after ACCA application, animals were decapitated, brains were rapidly removed onto a chilled brain matrix, and 2-mm-thick coronal slices were obtained. The slices were frozen on solid $CO_2$, and 1.5-mm-diameter punches were obtained from individual slices from the left hemisphere (where cannulae were placed). The punches were obtained from regions immediately below the cannula opening, that is, centered approximately 2 mm from the midline with the dorsal border tangential to the cortical-hippocampal fissure and contained elements of CA1, CA2, and CA3 as well as the dentate gyrus [31]. Frozen punches were transferred to microcentrifuge tubes and stored at −80°C until high-resolution magic angle spinning (HR-MAS) $^1$H magnetic resonance spectroscopy (MRS).

Frozen intact tissue samples were weighed (~2 mg) and placed directly into a Bruker zirconium rotor (4 mm in diameter, 10 μl in capacity) containing 5 μl of buffer (100 mM potassium phosphate, pH 7.4, 200 mM sodium formate, 1 g/L $NaN_3$, and 3 mM trimethylsilylpropionate) diluted with an equal volume of $D_2O$ containing 0.75% 3-(trimethylsilyl)-propionic acid (TSP). TSP serves as an internal chemical shift reference (0.00 ppm), formate (8.44 ppm) is used for phase corrections, whereas $D_2O$ is used to lock on the center frequency. The rotor (with sample) was placed into a Bruker magic angle spinning probe maintained at 4°C in a vertical wide-bore (8.9 cm) Bruker 11.7-T magnet with an AVANCE DRX-500 spectrometer (Bruker Biospin Corp, Billerica, MA). Rotors were spun at 4200 ± 2 Hz at 54.7 degrees relative to the static magnetic field $B_0$. Compensation of field inhomogeneities, pulse sequences, and signal acquisitions was carried out as described previously by us [32].

In brief, signals were acquired with Bruker XWINNMR (v 3.6 software) and the identical brain regions from all animals in an experimental cohort were analyzed in the same session. Spectra were analyzed with a custom LC Model software package (ver. 6.1-4) using a linear combination of 27 individual neurochemical model spectra (basis set) as well as nonspecific lipid signals to fit the tissue spectrum and calculate absolute concentration values for neurochemicals with signals between 1.0 and 4.2 ppm [33].

The precision of the LC Model fit to the spectral data was estimated with Cramér-Rao bounds; CRB were typically less than 10% and metabolites with CRB greater than 25% were not considered for further analysis. To account for variations in the mass of individual samples, absolute concentrations of MR-visible metabolites were corrected for tissue weight and expressed as nanomoles per milligram of wet tissue weight; variance associated with means suggests a substantial degree of analytical reproducibility [32].

### *Statistical Analysis*

Statistical analyses were carried out using SigmaPlot 9 program (Systat Software, San Jose, CA). Unless otherwise indicated, results are reported as mean ± SD. Survival was estimated using the Kaplan-Meier analytical method [34]. *P* values were calculated using

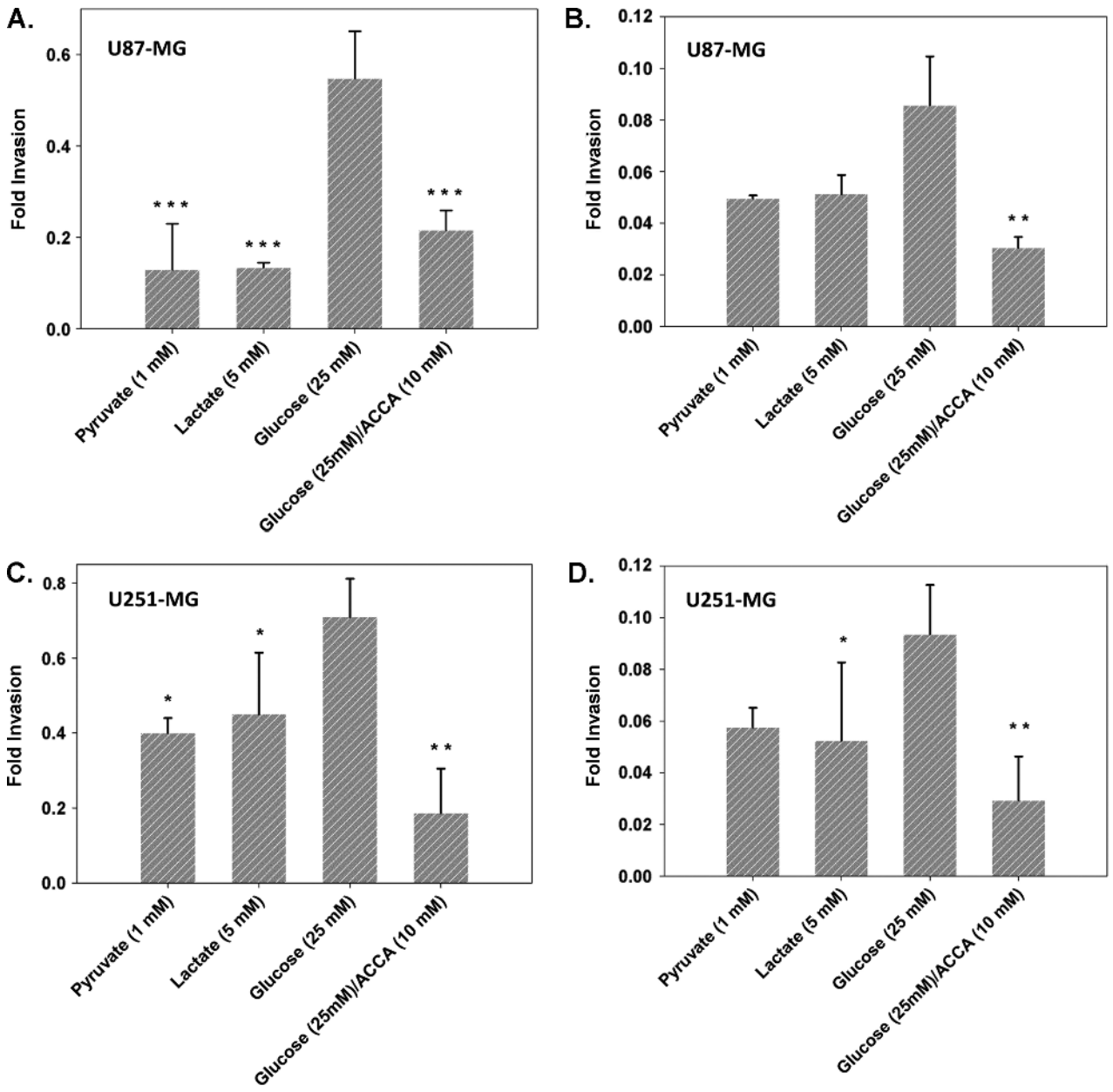


**Figure 1.** ACCA inhibits glucose mediated glioma invasiveness across Matrigel and organotypic brain slice cultures. Migration of EGFP-expressing glioma cells across Matrigel-coated transwell inserts or across 0.5-mm-thick coronal slices from the CPu region of immunodeficient rat brains were evaluated. Invasion across Matrigel of U87-MG (A) and U251-MG (C) ($n = 4$ per metabolite) or across coronal brain slices of U87-MG (B) and U251-MG (D) ($n = 4$ per metabolite) were plotted as fold invasion. Fold invasion = fluorescence of [(transwell bottom read) / (transwell top + bottom reads)]. Data shown as mean ± SEM. *P* values are indicated in comparison to glucose data. ***$P < .01$, **$.01 < P < .05$, *$.05 < P < .1$. Unmarked data sets had $.1 < P < .5$.

Student's *t* test or the Mann-Whitney rank sum test and considered statistically significant when $P < .05$. One-way analysis of variance with pairwise multiple comparisons (Holm-Sidak) was carried out for data analysis of invasion assays.

## Results

### *Glycolytic Flux Directly Modulates Glioblastoma Invasion*

Matrigel-based invasion assays have been the standard method to evaluate invasive capacity of tumor cells *in vitro*. We investigated the ability of glioma cells to invade across Matrigel under alternate metabolic stimuli and also analyzed the "invasiveness" of glioma cells in a setting more relevant in an *in vivo* environment using organotypic brain slice culture–based invasion assays. Comparison of the invasive capability of U87-MG and U251-MG glioma cells across both Matrigel and brain slice cultures indicated that 25 mM glucose enhanced invasive capacity over both pyruvate (1 mM) and lactate (5 mM) (Figure 1). Thus, enhancing glycolytic flux with glucose correlated with the ability of glioma cells to invade. However, supplementation of medium with lactate did not significantly stimulate invasive capacity, with invasive rates being mostly slightly higher than that for pyruvate. Despite this, when glucose-stimulated glioma cells were challenged with ACCA (to inhibit lactate efflux and collapse the glycolytic metabolism), we saw a significant two- to three-fold drop in the invasive capacity of the glioma cells, with the magnitude dropping to basal levels.

It should be noted that we chose 10 mM ACCA as the challenge concentration in the above experiments, as our previous *in vitro* studies [13] had indicated that, whereas 10 mM ACCA is inhibitory to lactate efflux, it does not result in apoptosis or necrosis of the glioma cells.

### *Extracellular Application of ACCA Does Not Impart Adverse Effects on Mitochondrial Respiration*

Previous studies by us using spectrophotometry have indicated that ACCA remains extracellular (thus does not directly impact mitochondrial pyruvate transport) unless the cell membranes are permeabilized (e.g., with digitonin) [13]. However, because of previous reports on impact of extracellular ACCA on mitochondrial respiration in intact tissue preparations [35], measurements were carried out to determine potential impact on mitochondrial respiration on *in vivo* application of ACCA. The results confirmed our prior spectrometric data and indicated that ACCA impacts mitochondrial respiration only on permeabilization of cells (Figure 2*A*). The respiratory rate remained unchanged on addition of ACCA, but subsequent addition of digitonin resulted in a brief respiratory burst most likely because of permeabilization of cells and exposure of mitochondria to respiratory substrates, followed by inhibition of respiration as ACCA blocked mitochondrial pyruvate entry (Figure 2*B*).

### *Convection-Enhanced Delivery of ACCA to the Tumor Bed Causes Necrosis of U87-MG Glioma*

Previous *in vitro* studies by us have indicated that 20 mM ACCA was sufficient to induce both apoptotic and necrotic cell death in U87-MG glioma cells, with approximately 70% cells becoming necrotic, whereas 10% cells remained apoptotic [13,36]. To test the *in vivo* efficacy of ACCA in killing glioma, we chose an orthotopic brain tumor nude rat model, in which ACCA was applied directly to the tumor bed. ACCA was continuously administered through CED [37–39] during a 28-day period to the center of the tumor using mini-

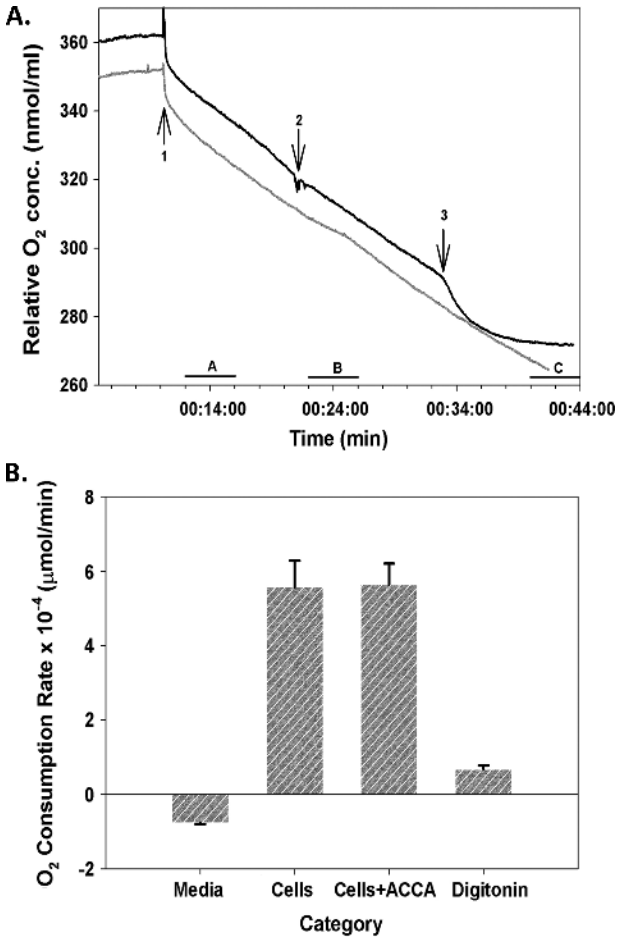


**Figure 2.** Extracellular ACCA does not inhibit $O_2$ consumption rate of U87-MG glioma cells. (A) Upper trace: Cells ($0.5 \times 10^6$) were added to DMEM/F12 medium maintained at room temperature (arrow 1) and rates of $O_2$ consumption traced for 10 minutes; ACCA was added to 10 mM final (arrow 2) and respiration measured for another 10 minutes, followed by addition of digitonin (40 $\mu$M final). Lower trace: $O_2$ consumption of cells incubated for a similar duration but in the absence of ACCA or digitonin. Lines A, B, and C mark the time intervals that were used to plot $O_2$ consumption rates ($n = 3$) at each step (B).

osmotic pumps (Alzet). In the first set of experiments, two alternate ACCA concentrations, namely, 20 and 40 mM, were tested first. When administered at 20 mM, the animals ($n = 3$) survived a mean of 48% longer than control animals that received saline in their osmotic pumps. Studies with 40 mM ACCA treated animals ($n = 3$) survived the longest (224%; $n = 2$), with the third animal indicating complete remission (necrosis) of the tumor (by MR imaging) and then surviving beyond the experimental end points even after the ACCA was exhausted in the osmotic pumps (Figure 3*A*).

Thereafter, we completed a second set of experiments with six animals per group using 40 mM ACCA only (Figure 3*B*). Of the test animals, three survived 212% longer than control animals that were treated with saline. MRI of the other three test animals indicated complete necrosis of tumor, and all three animals survived beyond the experimental end points (3 months after tumor implantation) with no recurrence of the tumor after ACCA was exhausted in the osmotic pumps (Figure 4, *A–D*). Thus, in this cohort, a 50% tumor-free survival rate was observed.

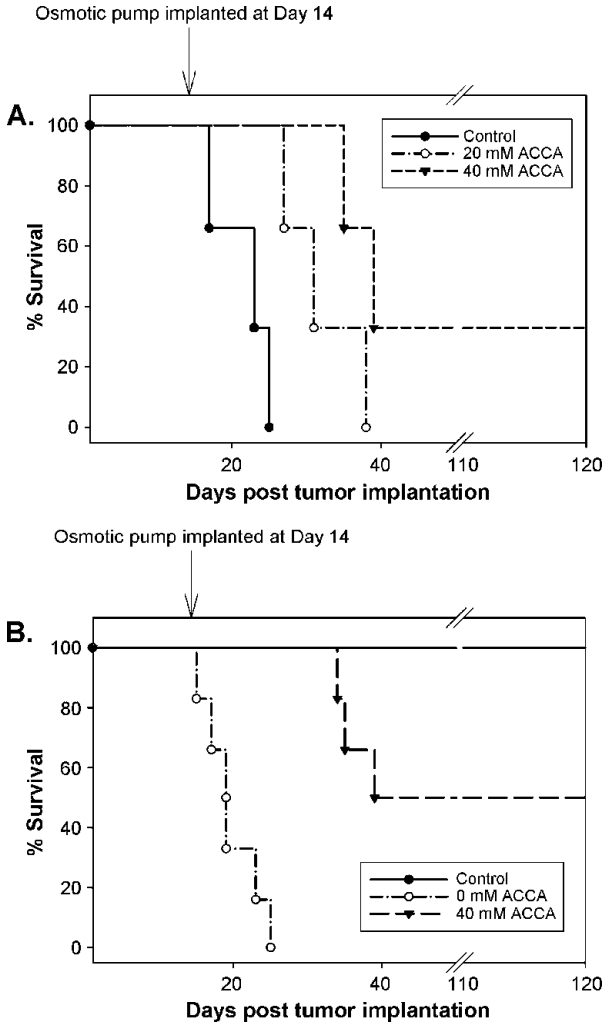


**Figure 3.** Kaplan-Meier survival analysis of immunodeficient rat orthotopic glioblastoma models treated with ACCA. (A) Animals implanted with glioma in the CPu region were subjected to CED with saline (control animals; $n = 3$) or ACCA at the indicated concentrations (test animals; $n = 3$ per group) and the survival followed up to 120 days. Day 1 = day of tumor implantation. (B) A second cohort of animals that were not implanted with tumor (control; $n = 3$) were administered 40 mM ACCA in the CPu region through CED to test for toxicity to ACCA. Two additional groups were implanted with glioma in the CPu region ($n = 6$ per group) at day 1 and treated with saline (0 mM ACCA) or 40 mM ACCA through CED 14 days after tumor implantation, and survival was monitored up to 120 days after tumor implantation.

### *Orthotopic Application of ACCA to Brains of Non–Tumor-Bearing Nude Rats through CED—While the Animals Displayed Normal Weight Gains and Lack of Tissue Necrosis at the Application Site, Altered Metabolic Profiles Were Observed in Adjacent Tissue*

One of our main concerns was that CED delivery of ACCA at mM concentrations may adversely impact the neuron-astrocyte lactate shuttle that is now recognized as crucial for normal neuronal function and metabolism [20,21]. To test, we cannulated the CPu region of non–tumor-bearing nude rats ($n = 6$ per group) in the same stereotaxic coordinates as those used for tumor implantation and applied either phosphate-buffered saline (Dulbecco PBS) or 40 mM ACCA through osmotic pumps at the same delivery rates as described previously. Animals were monitored daily up to 2 weeks after pump implantation to check for any observable neurologic deficits such as lack of grooming, mobility, gait, and gain or loss in body weight. Both control (Dulbecco PBS) and test (ACCA) animals showed normal behavioral patterns and their body weight gain/loss changes during the 2-week period did not deviate in a statistically significant manner ($P = .277$, Mann-Whitney rank sum test; $n = 3$ per group) (Figure 5), indicating lack of apparent toxicity on delivery of 40 mM ACCA to the brain through CED. At a superficial level, toxicity is not apparent when changes in body weight are compared with those of tumor-bearing rats ($n = 2$) where a continuous loss of body weight by 10% is initially indicated, until the animals begin responding to ACCA treatment ($P \leq .001$, Mann-Whitney rank sum test) (Figure 5). Furthermore, histologic (H&E) staining of coronal sections of the 40 mM ACCA-treated control animals did not indicate any tissue necrosis at the cannulation site

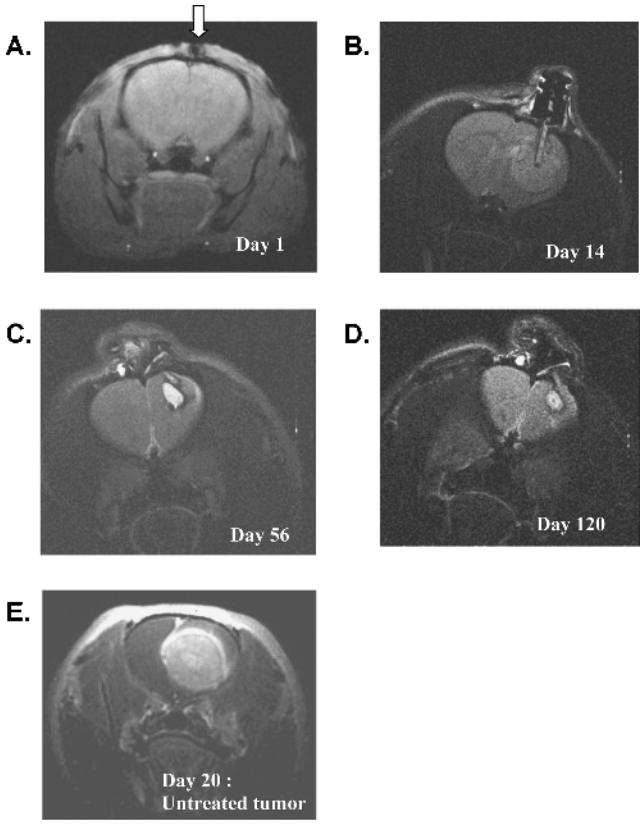


**Figure 4.** Coronal MR scans of immunodeficient rat orthotopic glioblastoma models treated with ACCA. Representative coronal MR scans of one of the six animals that survived beyond experimental end points is shown. Gadolinium contrast–enhanced images are shown at the cannulation point. (A) Day 1, immediately after implantation of tumor in the CPu region; the needle tract is indicated by arrow. (B–D) Images of the same coronal position at day 14 (day of osmotic pump implantation and cannulation of the tumor for CED of ACCA), day 56 (42 days after CED of ACCA and 14 days after exhaustion of ACCA in the osmotic pumps), and day 120 (106 days after CED of ACCA and 78 days after exhaustion of ACCA in the osmotic pump). Representative images of an animal that survived to day 120 are shown. (E) Tumor growth at day 20 in a representative animal that did not receive saline or ACCA through CED.

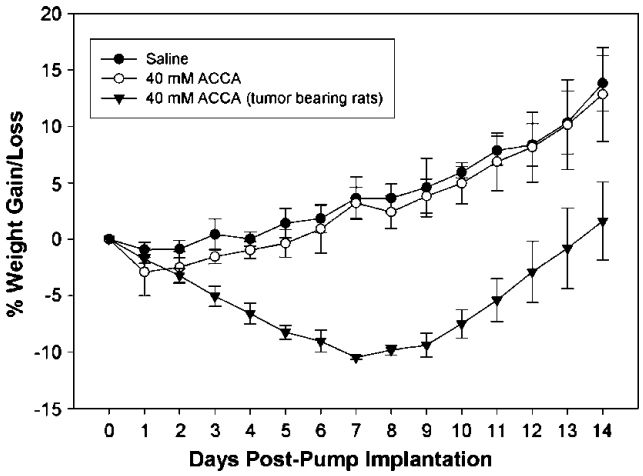


**Figure 5.** Percentage weight gain or loss in immunodeficient rats treated with 40 mM ACCA to the CPu region through CED. Non–tumor-bearing animals (weight, 300-350 g) were cannulated in the CPu region at the same stereotaxic location as for tumor implantation (day 0). Saline ($n = 3$) or 40 mM ACCA ($n = 3$) were delivered through osmotic pumps (28-day duration pumps; 200-$\mu$l capacity) for a period of 14 days, and the animals were weighed daily. The weight gain or loss of tumor-bearing animals that were treated with 40 mM ACCA through CED are shown for comparison ($n = 2$; day 0 = day of administration of 40 mM ACCA through CED, 14 days after tumor implantation).

(Figure 6). Histologic analysis of brains of tumor-implanted animals that survived beyond the experimental end points also indicated that, whereas complete necrosis of the tumor was observed, there was no visible damage to the surrounding normal brain tissues (Figure 7). For example, distinct signs of cellular necrosis including nuclear pyknosis or amorphous cytoplasmic staining (including cytolysis) [40] were not visible in the H&E micrographs. These results were also indicative of uniform and rapid dissemination of ACCA through CED, from the point of application into the tumor and then across the brain.

$^{1}$H MRS was carried out to further evaluate possible metabolic effects on the normal brain, where tissue punches from saline- or ACCA-treated animals ($n = 2$) were obtained (three punches per coronal slice, three slices per animal) immediately adjacent to the cannula opening. Of the 27 neurochemical basis set that was analyzed, 10 that had changes in concentration are listed in Table 1. Specific metabolic intermediates of the tricarboxylic acid cycle indicated altered metabolic profiles, including those derived from glutamate or aspartate. Glutamine, γ-aminobutyric acid, and succinate (derived from glutamate or downstream from glutamate in the tricarboxylic acid cycle) and *N*-acetyl aspartate and *N*-acetyl aspartylglutamate (derived from aspartate through oxaloacetate) showed statistically significant changes in their concentration profiles ($P < .05$). Lactate levels, which should be affected because of inhibition of plasma membrane MCTs by ACCA, also showed a reduction but at a lesser magnitude ($.05 < P < .1$).

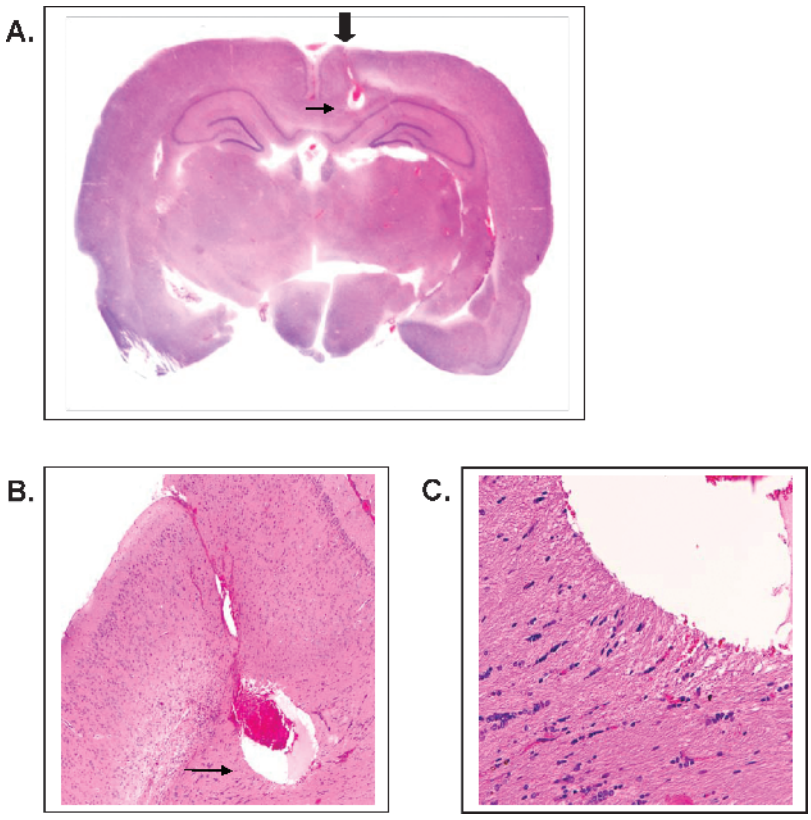


**Figure 6.** Histologic analysis of coronal sections of brains of immunodeficient rats treated with 40 mM ACCA through CED. (A) Representative H&E-stained coronal section (×10) of one of the animal brains that was evaluated for tissue necrosis at the cannulation point (cortical region; arrow) after CED of ACCA for 2 weeks. (B) Cannulation point (arrow) at ×40 magnification. (C) Cannulation point at ×200 magnification.

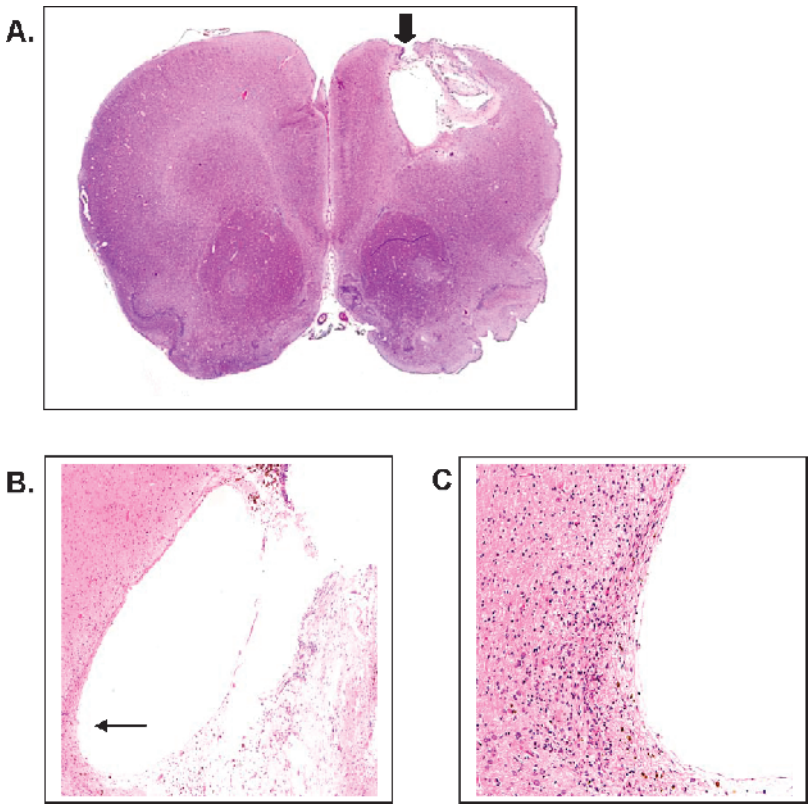


**Figure 7.** Histologic analysis of coronal sections of brains of tumor bearing rats after treatment with 40 mM ACCA through CED. (A) Representative H&E-stained coronal section (×10) of brain of one of the animals that survived beyond experimental end points. Cannulation/posttumor necrotic tissue cavity (striatal region; arrow) 120 days after CED of ACCA. (B) Necrotic cavity (arrow) at ×40 magnification. (C) Cavity wall at ×200 magnification.

### *Orthotopic CED of ACCA to the Brains of the Nude Rat Model Results in ACCA Concentration Gradients That Are Pharmacologically Relevant*

Next, we evaluated the *in situ* ACCA concentration gradients in the rat brains after a 2-week period of drug application through CED, using the same conditions as described in the previous paragraph. Coronal sections, 1.0 mm in thickness, were excised of the freshly isolated rat brains using a 0.5-mm brain matrix as described under Materials and Methods. ACCA concentrations in the clarified tissue homogenates were evaluated through HPLC-MS taking into account a mean brain tissue density of 1.04 [41]. The analyses indicated a maximum concentration of approximately 40 μM ACCA in the coronal sections (slice P1; Figure 8*A*) immediately posterior to the cannulated position (slice 0; Figure 8*A*), with concentration gradients dropping to 3 μM or less at distances of 5 to 6 mm from the point of application. Furthermore, levels of ACCA in the plasma from the above animals were below detection limits of the HPLC-MS when signal-to-noise ratios were normalized against control plasma from rats that were not exposed to ACCA.

## Discussion

Glioblastomas are the most malignant of brain tumors and, in common with most other highly malignant tumors, harbor aberrant metabolic pathways. Most recognized is their propensity to maintain an elevated glucose to lactic acid flux, necessitating the tumor to efflux lactic acid to the microenvironment. Thus, disruption of this last step (by inhibiting the MCTs that facilitate efflux) presents a "choke-point" that can be harnessed to destroy the glioblastoma preferably without affecting the surrounding normal brain tissue.

In this study, we used established glioblastoma cell lines to show that inhibition of lactate efflux in glioblastoma with α-cyano-4-hydroxy cinnamic acid (ACCA) will adversely impact both invasive and proliferative capacities of the tumor. Most significantly, we also show that ACCA, when applied directly to the tumor bed in an orthotopic brain tumor model through CED, can bring about complete tumor necrosis

**Table 1.** Alterations in Metabolic Profile of Normal Brain in Response to CED of ACCA to the Striatum.

| Metabolites | Application | |
|---|---|---|
| | Saline | ACCA (40 mM) |
| Creatine | 4.67 ± 0.24 | 4.00 ± 0.38 |
| γ-amino butyric acid | 2.22 ± 0.17 | 1.54 ± 0.08* |
| Glutamine | 2.43 ± 0.13 | 1.62 ± 0.17* |
| Glutamate | 7.57 ± 0.48 | 5.68 ± 0.61* |
| Glycerophosphoryl-choline | 0.85 ± 0.05 | 0.77 ± 0.09 |
| *myo*-inositol | 3.85 ± 0.23 | 3.47 ± 0.31 |
| Lactate | 7.46 ± 0.50 | 5.79 ± 0.73† |
| *N*-acetyl aspartate | 4.37 ± 0.30 | 3.24 ± 0.33* |
| *N*-acetyl aspartylglutamate | 1.11 ± 0.07 | 0.82 ± 0.05* |
| Succinate | 0.36 ± 0.03 | 0.23 ± 0.01* |

Metabolite concentrations are shown in nanomoles per milligram of wet tissue weight. Values are given as mean ± SEM.
*Statistically significant changes ($P < .05$) in metabolite concentrations.
†Changes with $.05 < P < .1$.

without causing damage to the surrounding normal brain tissues. A 50% survival rate was observed with the nude rat model with no tumor recurrence after treatment. Furthermore, we have determined the pharmacologically relevant ACCA concentration gradients that are established in the model to impart tumor necrosis.

Of the four known functional MCTs (MCTs 1-4) that transport lactate, all, except MCT3, are currently known to be overexpressed in tumors [8,42,43]. All four isoforms are expressed in normal brain with MCT1 and MCT4 predominating in astrocytes, whereas MCT2 is preferentially expressed in neurons [44,45]. MCT3 is located primarily in the choroid plexus and the retinal pigment epithelium [46]. Thus, a small-molecular inhibitor approach, as described in our studies, need to show partiality toward targeting the tumor while having minimal impact on the surrounding brain tissue, particularly on the astrocyte-neuron lactate shuttle that occurs between neurons and astrocytes during routine axonal firing [20,21].

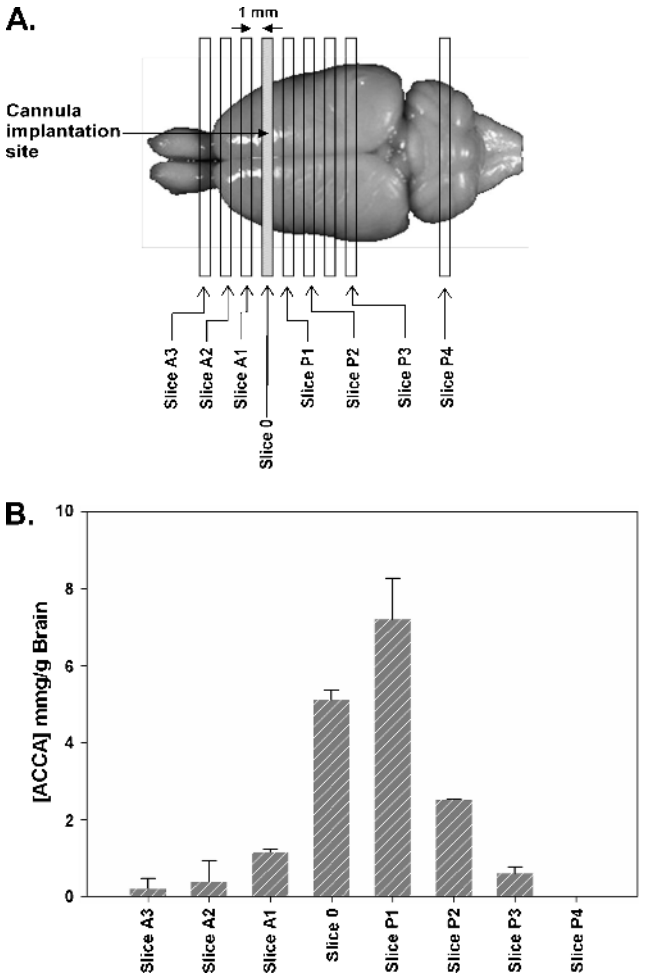


**Figure 8.** CED-mediated distribution of ACCA in immunodeficient rat brains. (A) Coronal brain sections, 1 mm in thickness, were obtained from animals that received 40 mM ACCA for 14 days through CED to the CPu region (non–tumor-bearing rats). Sections were weighed and processed for HPLC-MS analysis for ACCA concentration per slice. Slice 0 indicates cannulation point; slices A1–A3, anterior slices at 1-mm intervals from the cannulation point; slices P1–P3, posterior slices at 1-mm intervals from the cannulation point. (B) The ACCA concentrations (micrograms per gram of wet weight of brain) recorded were 0.195 ± 0.27 (A3), 0.0385 ± 0.54 (A2), 1.16 ± 0.06 (A1), 5.11 ± 0.24 (0), 7.21 ± 1.06 (P1), 2.52 ± 0.01 (P2), 0.595 ± 0.17 (P3).

We chose ACCA because it harbors a high $K_i$ (0.5 mM) against lactate transporters in tumors [17]. Although it is also known to inhibit pyruvate entry in isolated mitochondria [47], our current and previous *in vitro* studies have indicated that ACCA remains extracellular and thus should not impart adverse effects on mitochondrial pyruvate entry in intact cells [13]. Whereas small-molecule inhibitors of MCTs with higher affinity ($K_i$ of approximately 1-10 nM) have been reported recently [48–50], our primary concern was that such high-affinity inhibitors may also disrupt the neuron-astrocyte lactate shuttle. Thus, it was hoped that ACCA, with a higher $K_i$ (lower affinity toward MCTs), may have relatively low impact on the normal brain tissue while adversely affecting the highly elevated glycolytic metabolism of the glioblastoma.

Our previous *in vitro* studies have indicated that the glycolytic metabolism in these malignant tumors collapses on inhibition of lactate efflux [13,36]. In this report, our first goal was to identify whether inhibition of lactate efflux could adversely affect the glioblastoma's highly invasive nature. Our results with both Matrigel-based and brain slice culture–based invasion assays clearly indicated the inhibitory effects of ACCA on glioma invasion. The observed inability of 5 mM lactate to stimulate invasion at a magnitude similar to that with 25 mM glucose may be due to the use of lactate by the tumor cells toward their metabolism because the glioma cells were presented with only glutamine (2 mM) and 5 mM lactate as metabolic substrates in these "lactate" sample sets.

Both invasion assay methods showed similar fold inhibition of glucose-stimulated invasive capacity of glioblastoma cells by ACCA (supporting our hypothesis that disruption of lactate efflux by tumors will adversely affect invasive capacity). Our results may also indicate the importance of the stroma in modulating the invasiveness, a point expounded by other researchers [51]. For example, efflux of lactate by the tumor cells could directly modulate the stromal microenvironment to promote invasion rather than the mere enhancement of lactate levels around the tumor mass. Whereas it is known that tumor lactate can modulate extracellular matrix proteins in the tumor microenvironment [52,53], a recent report on glioma indicates that lactate can initiate a cascade of events to upregulate both expression and activity of transforming growth factor β and matrix metalloproteinase 2 and enhance the invasive capacity of glioma [54].

The above observations also correlate with the proton driven tumor invasion hypothesis proposed by Gatenby et al. [55–57], which was recently tested in a murine model using a bicarbonate-buffered system [58]. Thus, not only protons but also lactate are indicated to promote the invasiveness of tumors into the surrounding normal tissue environment. However, we cannot discount the possibility that collapse of glycolytic metabolism in the glioma cells (on inhibition of lactate efflux) may also have resulted in overall energy paucity in the tumor cells to contribute toward inhibition of invasive capacity.

Our primary concerns in a potential clinical applicability of metabolic targeting of glioma with ACCA or a similar drug were two-fold. First, from a pharmacological standpoint, ACCA had low potency (millimolar concentrations of ACCA were needed *in vitro* to cause necrosis in glioma) [13]. Second, *in vivo*, ACCA may interfere with the lactate shuttle between astrocytes and neurons and result in potentially lethal consequences.

Polar chemotherapeutics that target brain tumors are routinely and directly administered to the brain parenchyma surrounding the tumor

resection cavity to circumvent the blood-brain barrier, which effectively limits penetration by these drugs when applied through the systemic route [37]. We also chose direct application of ACCA to the tumor bed in our animal model because the molecule is anionic at physiological pH. To enhance diffusion of the drug throughout the tumor and the surrounding brain parenchyma, we applied the drug through CED by maintaining a pressure gradient through infusion with osmotic pumps. Application of ACCA directly to the tumor bed in our orthotopic nude rat brain tumor model resulted in highly promising results with a 50% survival rate when challenged with ACCA. In these surviving animals, the tumor had not recurred after 28 days of drug application (after the pumps "run dry"), and indicated complete necrosis of the tumor, which was verified by both MRI and histochemical staining. The surviving animals lived beyond the initially targeted experimental end points of 30 days after drug application and with normal weight gains and behavior/mobility.

The absence of adverse neurologic symptoms when naive (control) animals were challenged with orthotopic delivery of 40 mM ACCA through CED to the brain was also significant because it indicated that programmed delivery of low affinity lactate transporter inhibitors (even at millimolar concentrations) did not significantly affect brain function. Although these animals displayed normal weight gains and behavior, our $^{1}$H MRS analyses indicated that there were changes in the brain metabolite profiles due to CED of ACCA. Not surprisingly, the 2-week infusion of ACCA decreased lactate as well as other mitochondrial constituents such as *N*-acetyl aspartate, glutamate, and succinate. In the absence of any histologic evidence for neuronal death, decreases in these metabolic intermediaries suggest that neurons and glia, in contrast to tumor cells, have shifted to compensatory pathways to maintain energy equipoise.

The thousand-fold lower ACCA concentrations (10-40 μM) detected across the brain parenchyma and the lack of observable necrosis at cannulation points indicated that distribution of the drug is rapid through CED. Thus, pharmacologically applicable micromolar levels of ACCA had been sufficient to cause tumor necrosis in our studies. However, studies have indicated that serum factors such as albumin can bind ACCA and thus reduce the availability of the inhibitor at the tissue level [35]. Thus, the marked reduction in ACCA concentrations that was observed may be due to sequestration of ACCA by serum components. However, when the drug efflux rates by the osmotic pumps (0.25 μl/h) and the brain volumes (~2 ml per 400-g rat) of the experimental models are taken into consideration, a micromolar level of drug concentrations are feasible under steady-state conditions. Studies by others have indicated that CED at 1 μl/h can result in a drug diffusion radius of 0.5 cm from the cannula opening in a rat brain model [59].

Although ACCA was below detection limits in the systemic circulation, analysis of ACCA concentration across the brains along the sagittal plane indicated a normal distribution pattern, interestingly with slightly higher ACCA levels immediately posterior to the cannulation point. Whether the latter was due to influence of the anterior-to-posterior bulk CSF flow in the ventricular system needs to be determined.

Two previous studies have targeted the pyruvate–acetyl CoA–lactate metabolic axis of tumors with small-molecule drugs in rodent models. Decreased tumor size was reported in one study where dichloroacatate was provided *ad libitum* to channel the axis toward mitochondrial respiration (pyruvate to acetyl CoA) [60], with the studies currently advancing to clinical trial stage [61]. The other study examined intraperitoneal bolus application of ACCA against subcutaneously implanted breast tumors to show tumor growth inhibition and necrosis at the hypoxic tumor core [18]. In contrast, the studies we report here with the orthotopic brain tumor model show that programmed application of ACCA to the tumor bed through CED to the tumor bed will not only increase overall survival of the treated animals but also cause complete necrosis of the tumor in half of the treated animals with no recurrence. To the best of our knowledge, this is the first report on CED of MCT inhibiting small-molecule drugs to the tumor bed in a brain tumor (or solid tumor) model to demonstrate tumor necrosis with no recurrence in a subset of the treated animals. We also show that, while there is some impact on the profile of metabolic intermediaries in brain due to orthotopic delivery of these low-affinity (high-$K_i$) small-molecule inhibitors of lactate efflux, when administered through programmed delivery (CED) in an animal model, therapeutic results can still be achieved against brain tumors without major adverse neuropathologic effects, which have been a major concern in the tumor metabolism field.

In summary, our *ex vivo* and *in vivo* studies implicate the crucial nature of MCTs and lactate efflux to the survival and dissemination of tumors. The studies also indicate that intratumoral application of metabolic inhibitors of glycolysis through CED may be a promising avenue to target brain tumors in a future clinical setting, perhaps even before, or in the absence of, surgical debulking. Because malignant gliomas are highly heterogeneous, a therapy as envisaged above, where lactate efflux is cutoff by using MCT facilitated export as a "choke-point" will preclude the ability of these tumors cells to bypass this metabolic insult because alternative pathways do not exist to compensate and maintain the glycolytic flux, a metabolic facet critical for the tumor's survival.

## Acknowledgments

The authors thank Jing Li and Richard Wiegand of the Karmanos Cancer Institute Pharmacology Core for HPLC-MS analysis of the ACCA drug gradients in the drug applied rat brain sections, Seema Sethi of the Karmanos Cancer Institute Pathology Research Services for histopathologic examination of tissue sections, Ian Zitron for assistance with digital microscopy, Tom Owoc for digital photography, and L.P. Moragoda for reviewing the article.

## References

[1] Warburg O, Dickens F, and Kaiser Wilhelm-Institut fur Biologie B (1930). *The Metabolism of Tumours: Investigations from the Kaiser-Wilhelm Institute for Biology, Berlin-Dahlem.* Constable & Co, Ltd, London, UK.

[2] Baggetto LG (1992). Deviant energetic metabolism of glycolytic cancer cells. *Biochimie* **74**, 959–974.

[3] Pedersen PL (1978). Tumor mitochondria and the bioenergetics of cancer cells. *Prog Exp Tumor Res* **22**, 190–274.

[4] Walenta S, Schroeder T, and Mueller-Klieser W (2004). Lactate in solid malignant tumors: potential basis of a metabolic classification in clinical oncology. *Curr Med Chem* **11**, 2195–2204.

[5] Walenta S and Mueller-Klieser WF (2004). Lactate: mirror and motor of tumor malignancy. *Semin Radiat Oncol* **14**, 267–274.

[6] Halestrap AP and Price NT (1999). The proton-linked monocarboxylate transporter (MCT) family: structure, function and regulation. *Biochem J* **343**(Pt 2), 281–299.

[7] Halestrap AP and Meredith D (2004). The SLC16 gene family—from monocarboxylate transporters (MCTs) to aromatic amino acid transporters and beyond. *Pflugers Arch* **447**, 619–628.

[8] Mathupala SP, Parajuli P, and Sloan AE (2004). Silencing of monocarboxylate transporters via small interfering ribonucleic acid inhibits glycolysis and induces

cell death in malignant glioma: an *in vitro* study. *Neurosurgery* **55**, 1410–1419; discussion 1419.

[9] Froberg MK, Gerhart DZ, Enerson BE, Manivel C, Guzman-Paz M, Seacotte N, and Drewes LR (2001). Expression of monocarboxylate transporter MCT1 in normal and neoplastic human CNS tissues. *Neuroreport* **12**, 761–765.

[10] Mac M and Nalecz KA (2003). Expression of monocarboxylic acid transporters (MCT) in brain cells. Implication for branched chain α-ketoacids transport in neurons. *Neurochem Int* **43**, 305–309.

[11] Chiry O, Fishbein WN, Merezhinskaya N, Clarke S, Galuske R, Magistretti PJ, and Pellerin L (2008). Distribution of the monocarboxylate transporter MCT2 in human cerebral cortex: an immunohistochemical study. *Brain Res* **1226**, 61–69.

[12] Chiry O, Pellerin L, Monnet-Tschudi F, Fishbein WN, Merezhinskaya N, Magistretti PJ, and Clarke S (2006). Expression of the monocarboxylate transporter MCT1 in the adult human brain cortex. *Brain Res* **1070**, 65–70.

[13] Colen CB, Seraji-Bozorgzad N, Marples B, Galloway MP, Sloan AE, and Mathupala SP (2006). Metabolic remodeling of malignant gliomas for enhanced sensitization during radiotherapy: an *in vitro* study. *Neurosurgery* **59**, 1313–1323; discussion 1323–1314.

[14] Coss RA, Storck CW, Daskalakis C, Berd D, and Wahl ML (2003). Intracellular acidification abrogates the heat shock response and compromises survival of human melanoma cells. *Mol Cancer Ther* **2**, 383–388.

[15] Fang J, Quinones QJ, Holman TL, Morowitz MJ, Wang Q, Zhao H, Sivo F, Maris JM, and Wahl ML (2006). The $H^+$-linked monocarboxylate transporter (MCT1/SLC16A1): a potential therapeutic target for high-risk neuroblastoma. *Mol Pharmacol* **70**, 2108–2115.

[16] Mathupala SP, Colen CB, Parajuli P, and Sloan AE (2007). Lactate and malignant tumors: a therapeutic target at the end stage of glycolysis. *J Bioenerg Biomembr* **39**, 73–77.

[17] Spencer TL and Lehninger AL (1976). L-Lactate transport in Ehrlich ascites-tumour cells. *Biochem J* **154**, 405–414.

[18] Sonveaux P, Vegran F, Schroeder T, Wergin MC, Verrax J, Rabbani ZN, De Saedeleer CJ, Kennedy KM, Diepart C, Jordan BF, et al. (2008). Targeting lactate-fueled respiration selectively kills hypoxic tumor cells in mice. *J Clin Invest* **118**, 3930–3942.

[19] Sattler UG, Meyer SS, Quennet V, Hoerner C, Knoerzer H, Fabian C, Yaromina A, Zips D, Walenta S, Baumann M, et al. (2010). Glycolytic metabolism and tumour response to fractionated irradiation. *Radiother Oncol* **94**, 102–109.

[20] Pellerin L and Magistretti PJ (2004). Neuroscience. Let there be (NADH) light. *Science* **305**, 50–52.

[21] Kasischke KA, Vishwasrao HD, Fisher PJ, Zipfel WR, and Webb WW (2004). Neural activity triggers neuronal oxidative metabolism followed by astrocytic glycolysis. *Science* **305**, 99–103.

[22] Albini A, Iwamoto Y, Kleinman HK, Martin GR, Aaronson SA, Kozlowski JM, and McEwan RN (1987). A rapid *in vitro* assay for quantitating the invasive potential of tumor cells. *Cancer Res* **47**, 3239–3245.

[23] Platet N and Garcia M (1998). A new bioassay using transient transfection for invasion-related gene analysis. *Invasion Metastasis* **18**, 198–208.

[24] Jung S, Kim HW, Lee JH, Kang SS, Rhu HH, Jeong YI, Yang SY, Chung HY, Bae CS, Choi C, et al. (2002). Brain tumor invasion model system using organotypic brain-slice culture as an alternative to *in vivo* model. *J Cancer Res Clin Oncol* **128**, 469–476.

[25] Ohnishi T, Matsumura H, Izumoto S, Hiraga S, and Hayakawa T (1998). A novel model of glioma cell invasion using organotypic brain slice culture. *Cancer Res* **58**, 2935–2940.

[26] Mathupala SP (2001). Bicistronic Retroviral Vector pLXRN (Accession No. AF113968), GenBank. National Center for Biotechnology Information.

[27] Miller AD and Buttimore C (1986). Redesign of retrovirus packaging cell lines to avoid recombination leading to helper virus production. *Mol Cell Biol* **6**, 2895–2902.

[28] Miller AD, Trauber DR, and Buttimore C (1986). Factors involved in production of helper virus-free retrovirus vectors. *Somat Cell Mol Genet* **12**, 175–183.

[29] Paxinos G and Watson C (1998). *The Rat Brain in Stereotaxic Coordinates* (4th ed). Academic Press, San Diego, CA.

[30] Wiegand R, Wu J, Sha X, LoRusso P, Heath E, and Li J (2009). Validation and implementation of a liquid chromatography/tandem mass spectrometry assay to quantitate aminoflavone (NSC 686288) in human plasma. *J Chromatogr B Analyt Technol Biomed Life Sci* **877**, 1460–1464.

[31] Paxinos G and Watson C (2007). *The Rat Brain in Stereotaxic Coordinates* (6th ed). Academic Press/Elsevier, Amsterdam, Netherlands.

[32] Ghoddoussi F, Galloway MP, Jambekar A, Bame M, Needleman R, and Brusilow WS (2010). Methionine sulfoximine, an inhibitor of glutamine synthetase, lowers brain glutamine and glutamate in a mouse model of ALS. *J Neurol Sci* **290**, 41–47.

[33] Provencher SW (1993). Estimation of metabolite concentrations from localized *in vivo* proton NMR spectra. *Magn Reson Med* **30**, 672–679.

[34] Kaplan EL and Meier P (1958). Nonparametric estimator from incomplete observations. *J Am Stat Assoc* **53**, 457–481.

[35] Halestrap AP and Denton RM (1975). The specificity and metabolic implications of the inhibition of pyruvate transport in isolated mitochondria and intact tissue preparations by α-cyano-4-hydroxycinnamate and related compounds. *Biochem J* **148**, 97–106.

[36] Colen CB (2005). *Gene Therapy and Radiation of Malignant Glioma by Targeting Glioma Specific Lactate Transporter*. Neurological Surgery and Physiology, Wayne State University School of Medicine, Detroit, MI.

[37] Bobo RH, Laske DW, Akbasak A, Morrison PF, Dedrick RL, and Oldfield EH (1994). Convection-enhanced delivery of macromolecules in the brain. *Proc Natl Acad Sci USA* **91**, 2076–2080.

[38] Chen MY, Lonser RR, Morrison PF, Governale LS, and Oldfield EH (1999). Variables affecting convection-enhanced delivery to the striatum: a systematic examination of rate of infusion, cannula size, infusate concentration, and tissue-cannula sealing time. *J Neurosurg* **90**, 315–320.

[39] Degen JW, Walbridge S, Vortmeyer AO, Oldfield EH, and Lonser RR (2003). Safety and efficacy of convection-enhanced delivery of gemcitabine or carboplatin in a malignant glioma model in rats. *J Neurosurg* **99**, 893–898.

[40] Burkitt HG, Young B, Heath JW, and Wheater PR (1993). *Wheater's Functional Histology: A Text and Colour Atlas* (3rd ed). Churchill Livingstone, Edinburgh, UK.

[41] Gredell JA, Turnquist PA, MacIver MB, and Pearce RA (2004). Determination of diffusion and partition coefficients of propofol in rat brain tissue: implications for studies of drug action *in vitro*. *Br J Anaesth* **93**, 810–817.

[42] Wahl ML, Owen JA, Burd R, Herlands RA, Nogami SS, Rodeck U, Berd D, Leeper DB, and Owen CS (2002). Regulation of intracellular pH in human melanoma: potential therapeutic implications. *Mol Cancer Ther* **1**, 617–628.

[43] Pinheiro C, Reis RM, Ricardo S, Longatto-Filho A, Schmitt F, and Baltazar F (2010). Expression of monocarboxylate transporters 1, 2, and 4 in human tumours and their association with CD147 and CD44. *J Biomed Biotechnol* **2010**, 427694.

[44] Pierre K and Pellerin L (2005). Monocarboxylate transporters in the central nervous system: distribution, regulation and function. *J Neurochem* **94**, 1–14.

[45] Pellerin L, Bergersen LH, Halestrap AP, and Pierre K (2005). Cellular and subcellular distribution of monocarboxylate transporters in cultured brain cells and in the adult brain. *J Neurosci Res* **79**, 55–64.

[46] Philp NJ, Yoon H, and Lombardi L (2001). Mouse *MCT3* gene is expressed preferentially in retinal pigment and choroid plexus epithelia. *Am J Physiol Cell Physiol* **280**, C1319–C1326.

[47] Halestrap AP and Denton RM (1974). Specific inhibition of pyruvate transport in rat liver mitochondria and human erythrocytes by α-cyano-4-hydroxycinnamate. *Biochem J* **138**, 313–316.

[48] Hildyard JC, Ammala C, Dukes ID, Thomson SA, and Halestrap AP (2005). Identification and characterisation of a new class of highly specific and potent inhibitors of the mitochondrial pyruvate carrier. *Biochim Biophys Acta* **1707**, 221–230.

[49] Ovens MJ, Davies AJ, Wilson MC, Murray CM, and Halestrap AP (2010). AR-C155858 is a potent inhibitor of monocarboxylate transporters MCT1 and MCT2 that binds to an intracellular site involving transmembrane helices 7-10. *Biochem J* **425**, 523–530.

[50] Rae C, Nasrallah FA, and Broer S (2009). Metabolic effects of blocking lactate transport in brain cortical tissue slices using an inhibitor specific to MCT1 and MCT2. *Neurochem Res* **34**, 1783–1791.

[51] Valster A, Tran NL, Nakada M, Berens ME, Chan AY, and Symons M (2005). Cell migration and invasion assays. *Methods* **37**, 208–215.

[52] Stern R, Shuster S, Neudecker BA, and Formby B (2002). Lactate stimulates fibroblast expression of hyaluronan and CD44: the Warburg effect revisited. *Exp Cell Res* **276**, 24–31.

[53] Bellail AC, Hunter SB, Brat DJ, Tan C, and Van Meir EG (2004). Microregional extracellular matrix heterogeneity in brain modulates glioma cell invasion. *Int J Biochem Cell Biol* **36**, 1046–1069.

[54] Baumann F, Leukel P, Doerfelt A, Beier CP, Dettmer K, Oefner PJ, Kastenberger M, Kreutz M, Nickl-Jockschat T, Bogdahn U, et al. (2009). Lactate promotes

glioma migration by TGF-$\beta_2$–dependent regulation of matrix metalloproteinase-2. *Neuro Oncol* **11**, 368–380.

[55] Gatenby RA, Gawlinski ET, Gmitro AF, Kaylor B, and Gillies RJ (2006). Acid-mediated tumor invasion: a multidisciplinary study. *Cancer Res* **66**, 5216–5223.

[56] Smallbone K, Gatenby RA, Gillies RJ, Maini PK, and Gavaghan DJ (2007). Metabolic changes during carcinogenesis: potential impact on invasiveness. *J Theor Biol* **244**, 703–713.

[57] Gatenby RA and Gawlinski ET (2003). The glycolytic phenotype in carcinogenesis and tumor invasion: insights through mathematical models. *Cancer Res* **63**, 3847–3854.

[58] Robey IF, Baggett BK, Kirkpatrick ND, Roe DJ, Dosescu J, Sloane BF, Hashim AI, Morse DL, Raghunand N, Gatenby RA, et al. (2009). Bicarbonate increases tumor pH and inhibits spontaneous metastases. *Cancer Res* **69**, 2260–2268.

[59] Khan A, Jallo GI, Liu YJ, Carson BS Sr, and Guarnieri M (2005). Infusion rates and drug distribution in brain tumor models in rats. *J Neurosurg* **102**, 53–58.

[60] Bonnet S, Archer SL, Allalunis-Turner J, Haromy A, Beaulieu C, Thompson R, Lee CT, Lopaschuk GD, Puttagunta L, Harry G, et al. (2007). A mitochondria-$K^+$ channel axis is suppressed in cancer and its normalization promotes apoptosis and inhibits cancer growth. *Cancer Cell* **11**, 37–51.

[61] Michelakis ED, Sutendra G, Dromparis P, Webster L, Haromy A, Niven E, Maguire C, Gammer TL, Mackey JR, Fulton D, et al. (2010). Metabolic modulation of glioblastoma with dichloroacetate. *Sci Transl Med* **2**, 31ra34.